

Structural basis for ubiquitin recognition and autoubiquitination by Rabex-5

Sangho Lee¹, Yien Che Tsai^{2,4}, Rafael Mattera^{3,4}, William J Smith³, Michael S Kostelansky¹, Allan M Weissman², Juan S Bonifacino³ & James H Hurley¹

Rabex-5 is an exchange factor for Rab5, a master regulator of endosomal trafficking. Rabex-5 binds monoubiquitin, undergoes covalent ubiquitination and contains an intrinsic ubiquitin ligase activity, all of which require an N-terminal A20 zinc finger followed immediately by a helix. The structure of the N-terminal portion of Rabex-5 bound to ubiquitin at 2.5-Å resolution shows that Rabex-5–ubiquitin interactions occur at two sites. The first site is a new type of ubiquitin-binding domain, an inverted ubiquitin-interacting motif, which binds with ~29-μM affinity to the canonical Ile44 hydrophobic patch on ubiquitin. The second is a diaromatic patch on the A20 zinc finger, which binds with ~22-μM affinity to a polar region centered on Asp58 of ubiquitin. The A20 zinc-finger diaromatic patch mediates ubiquitin-ligase activity by directly recruiting a ubiquitin-loaded ubiquitin-conjugating enzyme.

The Rab GTPases are central regulators of vesicular trafficking and organelle identity in all eukaryotes^{1,2}. The Rab family is the largest branch of the Ras superfamily, comprising more than 60 members in mammalian cells. As with other small GTPases, the localization and activity of the Rab proteins is regulated by GTPase-activating proteins (GAPs), guanine-nucleotide dissociation inhibitors (GDIs) and guanine-nucleotide exchange factors (GEFs)^{3,4}. Rab GEFs promote the binding of GTP to Rab proteins, which in turn converts them to their active signaling conformation and stabilizes their binding to cellular membranes. The founding member of the Rab5 GEF family is the yeast vacuolar sorting protein Vps9 (ref. 5). Vps9 is the yeast ortholog of the human Rab5 GEF, Rabex-5. All Rab5 GEFs have in common a catalytic unit comprising a helical bundle and a Vps9-homology domain⁶. Most Rab5 GEFs do not function alone, but rather as components of larger multiprotein complexes, as exemplified by the Rabaptin-5–Rabex-5 complex^{7–10}.

Covalent monoubiquitination of proteins is a major regulatory signal in protein trafficking¹¹. In this process, the C-terminal carboxylate of a single molecule of the highly conserved 76-residue protein ubiquitin is covalently linked to a lysine residue in a substrate protein. This reaction is carried out by a series of enzymes known as E1, E2 and E3 (refs. 12–14). Monoubiquitination of many transmembrane cargo proteins marks them for sorting into endosomal pathways^{15–17}. Monoubiquitin moieties on these proteins are recognized by specific ubiquitin-binding domains in proteins of the trafficking machinery, including ubiquitin-interacting motifs (UIMs), coupling of unfolded protein response to endoplasmic reticulum-associated degradation

(CUE) domains, ubiquitin E2 variant (UEV) domains, and GGAs and TOM (GAT) domains¹⁸. UIMs are ~25-residue, single-helix motifs that were discovered through sequence analysis of the polyubiquitin-binding site in the proteasome subunit S5a¹⁹. UIMs bind monoubiquitin with 200–2,000 μM affinity (K_d)²⁰. Many trafficking proteins that contain UIMs and CUE domains are themselves monoubiquitinated in a manner that depends on both a ubiquitin ligase and the presence of the binding domain¹⁸. UIMs within epsin, eps15, eps15R and Vps27 (refs. 21–24) both bind monoubiquitin and promote their own monoubiquitination.

The yeast counterpart of Rabex-5, Vps9, contains a C-terminal CUE domain and is another well-characterized example of the monoubiquitination of a monoubiquitin-binding protein^{25–27}. It has been anticipated that Rabex-5 might also contain a C-terminal ubiquitin-binding domain²⁶, and a Rabex-5–ubiquitin interaction has been noted²⁷. However, the C-terminal segment of Rabex-5 does not bind ubiquitin²⁸. Rabex-5 interacts with ubiquitin, but does so through an N-terminal motif consisting of a zinc finger followed immediately by a 25-residue region predicted to form an α -helix²⁸.

The Rabex-5 N-terminal zinc finger belongs to the A20 zinc finger (A20 ZnF) family and has ubiquitin-ligase activity²⁸. The defining member of this family, A20, is a negative regulator of NF- κ B signaling that has both deubiquitinating (DUB)-enzyme and ubiquitin-ligase activities. A20 catalyzes the removal of a Lys63-linked polyubiquitin chain from the TNF receptor-1-binding protein RIP, followed by the ligation of a Lys48-linked polyubiquitin chain to RIP²⁹. The A20 protein contains seven A20 ZnF domains, and the fourth A20 ZnF is

¹Laboratory of Molecular Biology, National Institute of Diabetes and Digestive and Kidney Diseases, US National Institutes of Health (NIH), Bethesda, Maryland 20892, USA. ²Laboratory of Protein Dynamics and Signaling, National Cancer Institute-Frederick, NIH, Frederick, Maryland 21702, USA. ³Cell Biology and Metabolism Branch, National Institute of Child Health and Human Development, NIH, Bethesda, Maryland 20892, USA. ⁴These authors contributed equally to this work. Correspondence should be addressed to J.H.H. (hurley@helix.nih.gov).

Received 30 November 2005; accepted 17 January 2006; published online 5 February 2006; doi:10.1038/nsmb1064

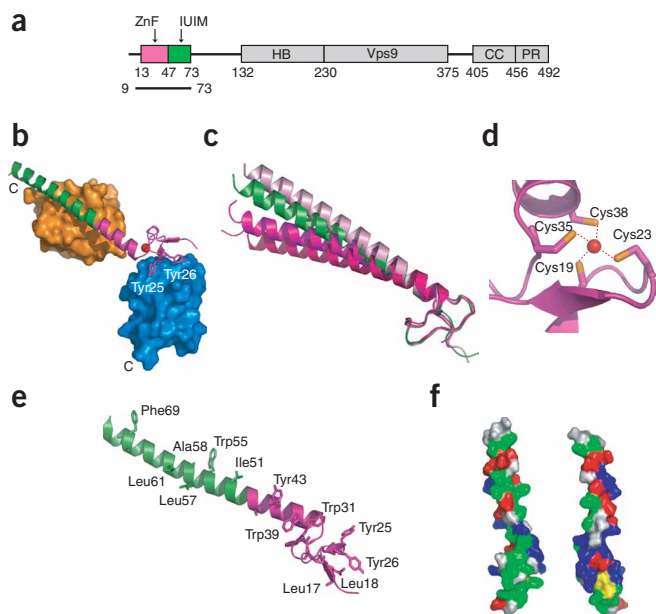


Figure 1 Structure of the Rabex-5 A20 ZnF domain and IUIM. **(a)** The domain structures of Rabex-5 and the construct used in this study. Magenta, ZnF domain; green, IUIM; HB, helical bundle; Vps9, Vps9-homology domain; CC, coiled coil; PR, proline-rich. **(b)** Rabex-5 (ribbon) contacts ubiquitin (orange and blue surfaces) at two sites in the crystal lattice. **(c)** Superposition of the four crystallographically independent molecules of the A20 ZnF domain and IUIM. Green, $P6_1$ molecule; pink, magenta and red, the three independent molecules in the asymmetric unit of the $C2$ lattice. **(d)** The zinc-binding site in the A20 ZnF domain. Orange, sulfurs of cysteine side chains; red sphere, zinc. **(e)** Ribbon and stick representation showing exposed hydrophobic side chains. **(f)** Surface of the A20 ZnF domain and IUIM colored by residue type: green, hydrophobic; red, acidic; blue, basic; white, uncharged polar; yellow, cysteine.

The $C2$ structure was determined by molecular replacement with the $P6_1$ structure. Together, the two crystal forms present images of four copies of the complex.

The structure reveals that the A20 ZnF and IUIM domains are fused into a single, relatively rigid unit (**Fig. 1b,c**). Residues 36–47 of the A20 ZnF, together with the entire IUIM, form a single contiguous helix. The nonhelical N-terminal part of the A20 ZnF contains three of the zinc ligands: Cys19, Cys23 and Cys35. The fourth zinc ligand, Cys38, is in the first turn of the helix (**Fig. 1d**). The zinc rigidly connects the nonhelical N-terminal part of the A20 ZnF with the helix. Trp31 of the nonhelical part of the A20 ZnF stacks against Trp39 of the helix, further stabilizing the orientation of the helix relative to the A20 ZnF (**Fig. 1e**).

The A20 ZnF has a notable hydrophobic patch on its surface, centered on a pair of hyperexposed residues, Tyr25 and Tyr26 (**Fig. 1e**). Leu17, Leu18, Trp31, Trp39 and Tyr43 are contiguous with the tyrosine pair, forming a 25-Å-long hydrophobic strip. The surface of the C-terminal portion of the IUIM helix presents a second hydrophobic strip, consisting of the exposed residues Ile51, Trp55,

required for the ubiquitin-ligase activity. Ubiquitin ligases identified previously fall into two classes. HECT-domain ligases form covalent thioesters with the ubiquitin C-terminal carboxylate and directly transfer ubiquitin to the lysine residues of substrate proteins^{12–14}. RING ligases contain a zinc-binding RING finger that interacts with substrate and with a ubiquitin-conjugating enzyme but does not form a covalent bond with the ubiquitin moiety to be transferred^{12–14}. The A20 ZnF domain represents a third class of ubiquitin ligase²⁹. Whereas the structural mechanisms for ubiquitin transfer through HECT-domain³⁰ and RING-domain³¹ ubiquitin ligases are well-studied, no structural information has been available for A20-domain ubiquitin ligases.

To better understand the mechanisms of Rabex-5 ubiquitin recognition and its A20 ZnF domain-based ubiquitin-ligase activity, we determined the crystal structure of the complex between bovine ubiquitin and the A20 ZnF and adjacent helix of bovine Rabex-5. The structure, together with surface plasmon resonance (SPR) and isothermal titration calorimetric (ITC) analyses, shows that both the Rabex-5 A20 ZnF domain and the helix adjacent to it bind ubiquitin with high affinity. This helix corresponds to an inverted IUIM, hence we refer to it as the IUIM throughout the remainder of this report. We go on to map the determinants for the ubiquitin-ligase activity to a hydrophobic patch on the surface of the A20 ZnF, providing a structural template for understanding the A20 ZnF class of ubiquitin ligases for the first time.

RESULTS

Structure of the Rabex-5 A20 ZnF and IUIM domains

The structure of Rabex-5 residues 9–73, comprising the A20 ZnF and IUIM domains (**Fig. 1a**), was determined in complex with ubiquitin at 2.8 Å in a $P6_1$ lattice containing one complex per asymmetric unit and at 2.5 Å in a $C2$ lattice containing three complexes per asymmetric unit. The structure was determined in $P6_1$ by molecular replacement, using ubiquitin as the search model. Density modification was used to determine the structure of the A20 ZnF–IUIM portion of the complex (**Supplementary Fig. 1** online). The structure of the complex in the $P6_1$ lattice was redetermined *de novo* by SAD using the native zinc ion, yielding a map consistent with the molecular-replacement solution.

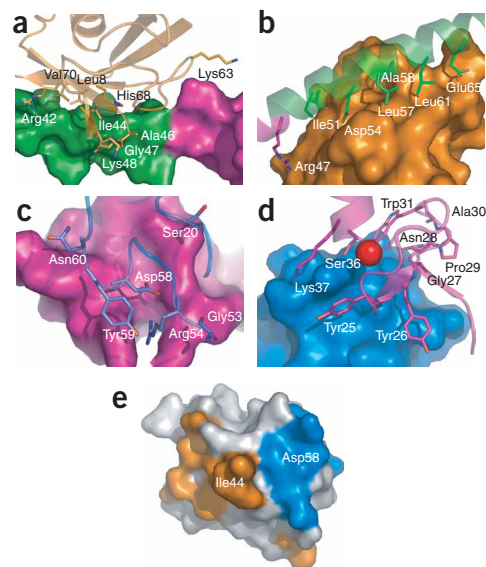


Figure 2 Ubiquitin recognition by Rabex-5. **(a)** Ubiquitin (beige ribbon and stick model) bound to Rabex-5 IUIM (green surface model). **(b)** Rabex-5 IUIM (green ribbon and sticks) bound to ubiquitin (orange surface). **(c)** Ubiquitin (blue ribbon and sticks) bound to Rabex-5 A20 ZnF domain (magenta surface). **(d)** Rabex-5 A20 ZnF domain (magenta ribbon and sticks) bound to ubiquitin (blue surface). **(e)** Ubiquitin binds Rabex-5 through two different nonoverlapping surfaces on ubiquitin. Orange, surfaces contacting the IUIM; blue, surfaces contacting the A20 ZnF.

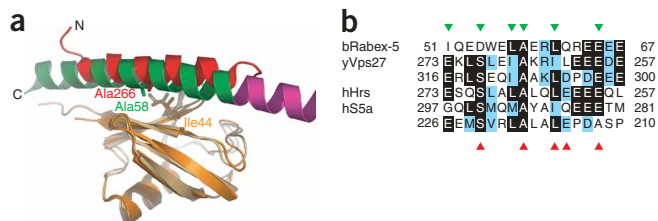


Figure 3 Conservation of IUIMs and their relationship to UIMs. (a) Superposition of Rabex-5 IUIM (green) and Vps27 UIM (red; PDB entry 1Q0W) on the basis of overlaid ubiquitin molecules (orange and beige). (b) Sequence of bovine Rabex-5 (bRabex-5) IUIM aligned with secondary structure elements of the UIMs of yeast Vps27 (yVps27), human hepatocyte growth factor receptor substrate (hHrs, the human Vps27 ortholog) and human proteasome subunit S5a (hS5a). The latter three sequences are written from C terminus to N terminus. Residues contacting ubiquitin are marked with green (IUIM) and red (Vps27 UIM-1) triangles, respectively.

Leu57, Ala58, Leu61 and Phe69 (Fig. 1e,f). This IUIM hydrophobic strip is flanked by the acidic residues Glu53, Asp54, Glu56, Glu59, Glu64, Glu65, Glu66 and Glu67.

Structure of the Rabex-5–ubiquitin complex

Ubiquitin and the Rabex-5_{9–73} fragment are present at 1:1 stoichiometry in both lattices. The complex is packed so that the two molecules interact at two distinct interfaces in both lattices. In the first interface, ubiquitin binds Rabex-5 through the Rabex-5 IUIM. Ubiquitin binds through its surface hydrophobic patch centered on Ile44, Leu8 and Val70 (Fig. 2a). The ubiquitin-binding site in the IUIM is centered on Ile57 and Ala58, and it includes all of the hydrophobic strip on the IUIM (Fig. 2b). There are hydrogen bonds between the side chain of Rabex-5 Arg47 and the main chain carbonyl of ubiquitin Lys63, and between the side chain of Rabex-5 Asp54 and the main chain amides of ubiquitin Ala46 and Gly47, and there is a salt bridge between Rabex-5 Glu65 and ubiquitin Arg42 (Supplementary Fig. 1). Two potential sites of ubiquitin-chain extension, Lys48 and Lys63, are near the interface (7–9 Å from the lysine N ζ to the nearest Rabex-5 atom; Fig. 2a). Both lysines are solvent accessible in the complex. The shape-complementarity score³² is 0.76, highly complementary. The complex buries 780 Å² and 710 Å² of the solvent-accessible surface areas on Rabex-5 and ubiquitin, respectively.

The A20 ZnF of Rabex-5 forms a second interface with a molecule of ubiquitin that is distinct from the one bound to the IUIM (Fig. 2c–e). At closest approach, these two ubiquitin molecules are 20 Å apart. Tyr25 and Tyr26 of the A20 ZnF hydrophobic patch are the main locus of the interaction. A20 ZnF Asn28, Trp31, Ser36 and Lys37 also interact (Fig. 2d). The interaction site on ubiquitin consists of the polar residues Arg54, Thr55, Ser57, Asp58, Tyr59 and Asn60 (Fig. 2c). Aliphatic and aromatic carbon atoms on these side chains interact with the di-tyrosine motif on the A20 ZnF domain. Rabex-5 Ser36 forms two hydrogen bonds with ubiquitin Asp58 (Supplementary Fig. 1). The shape-complementarity score is 0.74, nearly identical to the high score obtained for the ubiquitin-IUIM interaction. Roughly 420 Å² of solvent-accessible surface area is buried on each molecule.

Rabex-5 contains an inverted UIM

The IUIM of Rabex-5 binds the Ile44 patch on ubiquitin in a manner akin to the Vps27 UIM-1 (ref. 33). The Rabex-5 and Vps27 UIM-1 (PDB entry 1Q0W) complexes were superimposed via the ubiquitin molecules (Fig. 3a). Vps27 residues 257–275 are helical and in contact

with the same surface on ubiquitin as are Rabex-5 residues 49–67. The conserved central Ala266 of the Vps27 UIM-1 corresponds to the central Ala58 of the Rabex-5 IUIM (Fig. 3b). There is a one-to-one correspondence between ubiquitin-interacting residues in the C-terminal two-thirds of the Rabex-5 IUIM and the N-terminal two-thirds of the Vps27 UIM-1. The relationship breaks down only for the N-terminal five residues of Rabex-5. Asp54 of Rabex-5 makes interactions with the main chains of ubiquitin residues 46 and 47 much like those reported for its counterpart in Vps27, the conserved Ser270 (ref. 33). For this reason, we designated the Rabex-5 ubiquitin-binding helix an ‘inverted ubiquitin-interacting motif’ (IUIM).

A template for the A20 ZnF family

The A20 ZnF is a compact unit built around two pairs of cysteine residues and a single zinc ion. The coordination of the zinc by four cysteines (Fig. 1d) and the helical conformation of the last cysteine fit the pattern of the classic CCCC finger³⁴. This class of zinc finger is found in the GATA, LIM and PHD domain-containing DNA-binding proteins, the C1 and FYVE domain-containing peripheral membrane proteins and the first zinc site in the RING-domain ubiquitin ligases³⁴. The key Tyr-Tyr pair corresponds to phenylalanine or tyrosine in the sequences of other A20 ZnF domains (Fig. 4a) and is surrounded by other conserved residues (Fig. 4b). The A20 ZnF was overlaid on the Cbl RING structure on the basis of the similarity between the A20 zinc site and the first zinc site in the RING domain (data not shown). The UbcH7-binding site on the Cbl RING domain³¹ overlays a nonconserved polar surface on A20 distal to the Tyr-Tyr patch. This is consistent with the classification of the A20 ZnF ubiquitin ligases as a separate group from the RING ubiquitin ligases. Another zinc finger domain, the NZF domain, also binds ubiquitin. The NZF domain contains no α -helix and binds ubiquitin through its Ile44 patch³⁵, and it thus has little in common with the A20 zinc finger.

Mutational analysis of ubiquitin-binding sites

To evaluate the contribution of the A20 ZnF and IUIM regions to ubiquitin binding, residues in these regions were mutagenized

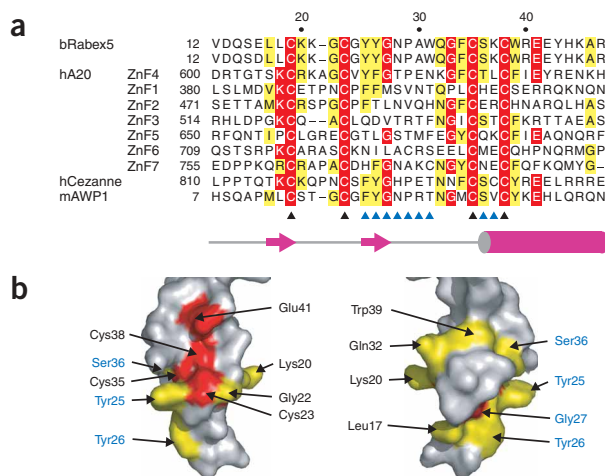


Figure 4 Conservation of A20 ZnF domains. (a) Structure-based sequence alignment of A20 zinc fingers. b, bovine; h, human; m, murine; AWP1, associated with PRK1; black triangles at bottom, conserved cysteine residues; blue triangles, ubiquitin-binding residues. Sequence numbering is for bovine Rabex-5. (b) Surface of the Rabex-5 A20 ZnF colored by conservation. Red, strictly conserved; yellow, highly conserved; blue, ubiquitin-binding residues.

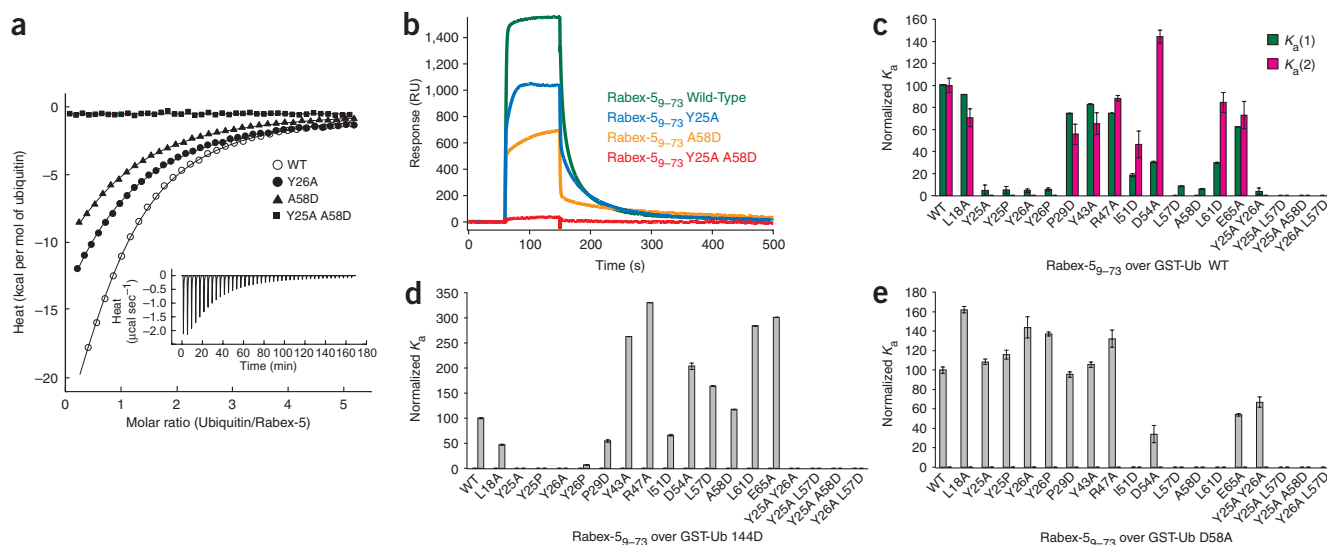


Figure 5 The ubiquitin–Rabex-5 interaction *in vitro*. **(a)** ITC analysis of the binding of ubiquitin to the Rabex-5₉₋₇₃ constructs *in vitro*. Inset, raw heat change elicited by successive injections of ubiquitin into a solution of wild-type (WT) Rabex-5₉₋₇₃. Main chart, the normalized integration data as a function of the molar ratio of ubiquitin to the various Rabex-5₉₋₇₃ constructs. Results shown are typical of four independent experiments carried out with the wild-type construct and two independent experiments carried out with each individual mutant. **(b)** SPR sensorgrams for selected Rabex-5₉₋₇₃ mutants with immobilized wild-type GST-ubiquitin. **(c–e)** Histograms showing relative affinities of Rabex-5₉₋₇₃ mutants for wild-type **(c)**, I44D **(d)** and D58A **(e)** GST-ubiquitin. Error bars show s.d. K_a values were obtained by taking the inverse of K_d values from **Table 1** and normalized by setting K_a for wild-type Rabex-5₉₋₇₃ to 100. A two-site model was used to fit the data for wild-type GST-ubiquitin **(c)** and a one-site model was used for I44D **(d)** and D58A **(e)**. Values greater than 100 in panels **c–e** probably reflect the limitations of the simple one- and two-site models used to fit the data rather than real increases in affinity.

individually and in combination. ITC was used to determine the effects on binding to ubiquitin in free solution (**Fig. 5a**). SPR was used to determine the effect on binding to ubiquitin immobilized on a planar surface (**Fig. 5b**). Wild-type Rabex-5₉₋₇₃ binds ubiquitin in solution with an apparent K_d of 12 μM when the ITC data are fit assuming there is only one type of binding site. These data fits had high residuals, suggesting that the single-site model was inappropriate. It was not possible to obtain substantial improvement by fitting the ITC data to a two-site model, so we pursued a mutational approach instead. The mutations L57D and A58D in the IUIM reduced affinity to $K_d = 22$ and 21 μM , respectively. The mutation Y26A reduced affinity to $K_d = 29$ μM . The double mutation Y25A A58D completely abolished binding at achievable concentrations. From these results, we infer that the most deleterious point mutations in each site are capable of completely abrogating binding to that site. We infer that the A20 site has a K_d of ~ 21 μM and the IUIM site has a K_d of ~ 29 μM in free solution.

Wild-type Rabex-5₉₋₇₃ binds immobilized ubiquitin with apparent K_d s of 1.3 μM and 37 μM when the SPR data are fit with a two-site model (**Fig. 5c** and **Table 1**). Glutathione *S*-transferase (GST)-ubiquitin was immobilized on the sensor chip. As GST is a dimer, two ubiquitin molecules are presented to the Rabex-5 molecule on average. The higher apparent affinity of wild-type Rabex-5₉₋₇₃ for dimeric immobilized ubiquitin compared to that for ubiquitin in solution suggests that avidity has a role in the former case. The most deleterious mutation in the A20 ZnF domain, Y25A, resulted in $K_d = 29$ μM , and that in the IUIM, A58D, resulted in $K_d = 22$ μM . The mutant Y25A A58D had no detectable binding. The SPR data suggest that the A20 ZnF and IUIM sites have K_d values of ~ 22 and 29 μM , respectively. The agreement between the ITC and SPR results for the two sites is excellent, given the differences in the presentation of the molecules in the two experiments.

To determine which interfaces of ubiquitin are involved in function, the ubiquitin mutants I44D and D58A were generated and the binding of these mutants to wild-type and mutant Rabex-5 constructs was assessed. The I44D mutation was made to disrupt the canonical hydrophobic patch on the surface of ubiquitin that interacts with the IUIM. The ubiquitin D58A mutation was designed to disrupt the two hydrogen bonds between ubiquitin Asp58 and the Rabex-5 Ser36 side chain and main chain. Ubiquitin I44D binds wild-type Rabex-5 and its IUIM mutant A58D with very similar affinities ($K_d = 20$ –23 μM ; **Fig. 5d** and **Table 1**). This is consistent with the expectation that either mutation should completely abrogate the Rabex-5 IUIM–ubiquitin Ile44 patch interaction, yet have no effect on the A20 ZnF–ubiquitin Asp58 patch interaction. Ubiquitin I44D binds with sharply reduced affinity to Rabex-5 A20 ZnF-domain mutant Y25A and not at all to Y25A Y26A. This confirms that the residual interaction of I44D with Rabex-5 requires an intact binding site in the A20 ZnF domain. Ubiquitin D58A binds wild-type Rabex-5 and its A20 ZnF-domain mutant Y25A with very similar affinities ($K_d = 26$ –28 μM ; **Fig. 5e** and **Table 1**), consistent with the structural finding that these two regions directly interact. In contrast, mutating the Rabex-5 IUIM (A58D) almost completely blocks binding. Thus, the residual Rabex-5 binding of the D58A mutant occurs entirely through the IUIM. These results show that both of the ubiquitin–Rabex-5 interfaces seen in the crystal structure are functional.

Mechanism for ubiquitin-ligase activity

To probe the mechanism for ubiquitin-ligase activity by Rabex-5, we tested the ability of Rabex-5₉₋₇₃ and its A20 ZnF-domain mutant Y25A Y26A to recruit ubiquitin-conjugating enzymes (Ubc; **Fig. 6a**). Both ubiquitin-loaded and non-ubiquitin-loaded human UbcH5C and *Mus musculus* Ubc7 (also called Ube2g2) were tested. To assess specificity, Rabex-5 was compared to the Ube2g2-binding protein, gp78

Table 1 Binding affinities of Rabex-5₉₋₇₃ for ubiquitin

Rabex-5 ₉₋₇₃	SPR ^a				ITC ^b
	GST-ubiquitin WT		GST-ubiquitin I44D	GST-ubiquitin D58A	
	<i>K</i> _{d1} (μM)	<i>K</i> _{d2} (μM)	<i>K</i> _d (app) ^c (μM)	<i>K</i> _d (app) ^c (μM)	Ubiquitin WT <i>K</i> _d (app) ^c (μM)
WT	1.3 ± 0.2	37 ± 6.7	23 ± 0.8	28 ± 3.3	12 ± 1
L18D	1.4 ± 0.1	52 ± 8.1	49 ± 1.3	17 ± 3.3	
Y25A	29 ± 4.8	NA ^d	ND ^e	26 ± 2.8	
Y25P	26 ± 3.1	NA ^d	ND ^e	24 ± 4.7	
Y26A	30 ± 1.5	NA ^d	ND ^e	20 ± 11	29 ± 1
Y26P	24 ± 1.4	NA ^d	ND ^e	21 ± 1.9	
P29D	1.8 ± 0.1	66 ± 9.3	42 ± 2.8	30 ± 2.8	
Y43A	1.6 ± 0.1	56 ± 10	8.8 ± 0.3	27 ± 2.8	14
R47A	1.8 ± 0.05	42 ± 2.5	7 ± 0.4	21 ± 8.9	
I51D	7.1 ± 1.5	79 ± 12	35 ± 1.2	ND ^e	
D54A	4.3 ± 0.6	25 ± 5.8	11 ± 6.4	83 ± 8.9	19 ± 1
L57D	15 ± 0.3	NA ^d	14 ± 0.4	ND ^d	22 ± 3
A58D	22 ± 0.4	NA ^d	20 ± 0.4	ND ^d	21 ± 1
L61D	4.4 ± 0.5	43 ± 9.1	8.1 ± 0.3	ND ^d	15
E65A	2.1 ± 0.1	50 ± 12	7.7 ± 0.2	53 ± 1.3	29 ± 1
Y25A Y26A	36 ± 3	NA ^d	ND ^e	42 ± 5.3	
Y25A L57D	ND ^e	ND ^e	ND ^e	ND ^e	
Y25A A58D	ND ^e	ND ^e	ND ^e	ND ^e	ND ^e
Y26A L57D	ND ^e	ND ^e	ND ^e	ND ^e	

^aFor SPR experiments, wild-type (WT) and mutant human GST-ubiquitin were immobilized on a CM5 chip. WT and mutant Rabex-5₉₋₇₃ were in the mobile phase. Means and standard deviations from three independent experiments are shown. ^bFor ITC experiments, bovine ubiquitin was titrated to WT and mutant Rabex-5₉₋₇₃. Shown are means and standard deviations from four independent experiments for wild-type protein and two independent experiments for mutants, except for Y43A and L61D, which were each measured once. ^cApparent dissociation constant calculated from fitting the data to a one-site model. ^dNA, binding seems to most appropriately fit a single-site model, so no *K*_{d2} was determined. ^eND, either binding was not detectable or the *K*_d was not determined because binding was too weak to obtain reliable quantification.

(ref. 36) and the UbcH5C-binding E3, RNF25 (ref. 37). Ubiquitin-loaded UbcH5C binds wild-type Rabex-5₉₋₇₃, but not the A20 ZnF domain Y25A Y26A mutant or gp78 (Fig. 6a). Non-ubiquitin-loaded UbcH5C does not bind Rabex-5₉₋₇₃. Ube2g2 binds gp78 with roughly equal affinities in both its ubiquitin-loaded and non-ubiquitin-loaded states (Fig. 6a). Thus, Rabex-5 specifically recruits at least one Ubc,

The conserved serine of the conventional UIM is replaced by an aspartate in the IUIM, in one of the few differences. However, the serine and the aspartate both interact with the same main chain NH groups on ubiquitin. It is equally notable that the orientation of the helix with respect to the ubiquitin surface, apart from its opposite N-to-C direction, is so similar. This suggests

Ubch5C, in a manner that depends on the interaction between ubiquitin and the A20 ZnF domain. The presence of ubiquitin alone is insufficient, at least at concentrations tested, as ubiquitin-loaded Ubc2g2 is not recruited. The ubiquitin-ligase activity with respect to GST-Rabex-5₉₋₇₃ was also tested. The A20 ZnF-domain tyrosine mutations that we tested blocked catalytic activity, consistent with the requirement for Ubc binding (Fig. 6b). The IUIM mutation A58D did not block activity, but rather enhanced activity several-fold.

DISCUSSION

The structure of the Rabex-5 IUIM is a striking illustration of convergent evolution. The GATA-like CCCC zinc fingers, of which the A20 ZnF is a subtype, all contain a C-terminal α-helix. The extension of this helix for Rabex-5 seems a likely mechanism for the origin of the IUIM. It is remarkable that the use of particular amino acid side chains to interact with particular ubiquitin residues is so well preserved. Key Rabex-5 IUIM alanine and leucine residues have alanine and leucine or isoleucine counterparts in conventional UIMs that make nearly identical interactions. The cluster of acidic residues at the C terminus of the IUIM is matched by a similar cluster at the N terminus of the UIM.

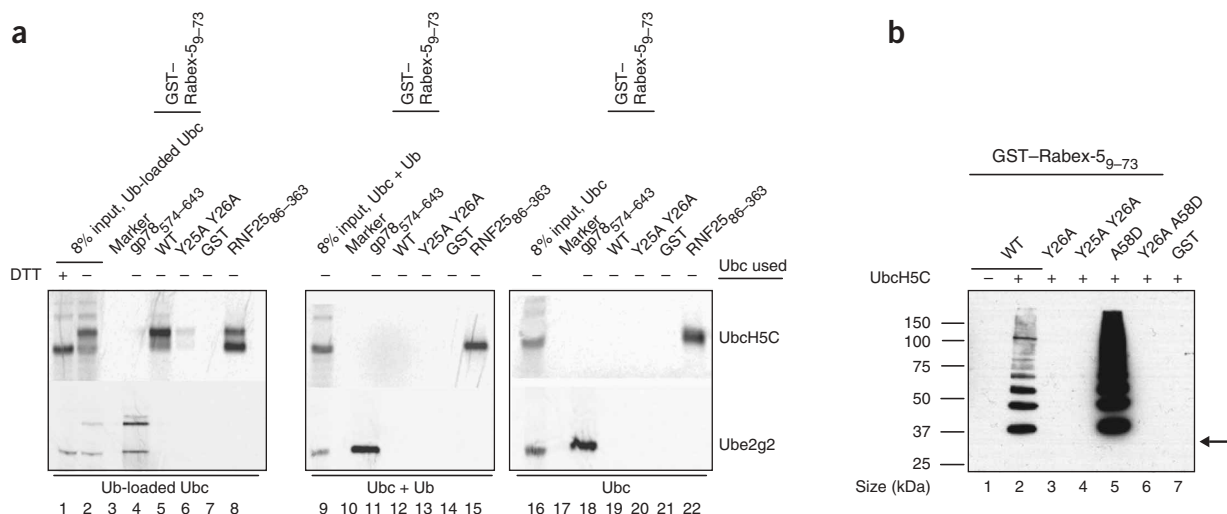


Figure 6 Ubc recruitment and ubiquitin-ligase activity of Rabex-5 and its mutants. **(a)** Detection of ³⁵S-labeled Ubcs shows that ubiquitin-loaded UbcH5C selectively binds Rabex-5 with an intact A20 ZnF domain, but not the Y25A Y26A Rabex-5 mutant. Ube2g2 binds the Ubc-binding domain of gp78 independently of its ubiquitin loading and does not bind Rabex-5. **(b)** Wild-type Rabex-5 has ubiquitin-ligase activity, as indicated by detection of Flag-ubiquitin. Tyrosine mutations in the A20 ZnF domain block this activity, whereas the A58D IUIM mutation enhances activity. Arrow marks the position corresponding to the molecular weight of unmodified GST-Rabex-5₉₋₇₃.

that there may be very few ways for a single α -helix to bind ubiquitin with substantial affinity.

Most monoubiquitin-binding domains bind free ubiquitin with K_d values ranging from 100–500 μM ¹⁸. By the standards of monoubiquitin-binding domains, the Rabex-5 IUIM is an unusually strong binder with its apparent K_d of $\sim 29 \mu\text{M}$. The Rabex-5 IUIM joins the Vps9 CUE domain^{25,38} as a ‘champion’ monoubiquitin binder. It is probably no coincidence that two of the most potent monoubiquitin-binding proteins described are orthologs. What is more noteworthy is that Rabex-5 and Vps9, despite their similar catalytic domains and biological functions, have evolved completely different high-affinity ubiquitin-binding domains located in completely different parts of their sequences. How does the Rabex-5 IUIM achieve such high-affinity binding as compared to conventional UIMs and most other ubiquitin-binding domains? The surface area buried in the ubiquitin-IUIM interface, over 700 \AA^2 for each protein, is comparable to that buried in the high-affinity Vps9 CUE-ubiquitin interface and larger than that of most other ubiquitin-domain interfaces. Compared to the UIM, the IUIM interacts with one additional turn of helix that forms hydrogen bonds with the Lys63 region of ubiquitin. These interactions could contribute 2 kcal mol⁻¹ and account for the ~ 10 -fold gain in affinity compared to the Vps27 UIM-1.

Monoubiquitin-binding domains in many proteins, including eps15, epsin, Vps27, Vps9 and Rabex-5, are required for the covalent monoubiquitination of these proteins. The mechanism by which monoubiquitin-binding domains promote ubiquitination is unknown, although several models have been proposed¹⁸. In one model²¹, the UIM directly recruits a covalent HECT-domain ubiquitin ligase-ubiquitin thiolester adduct via the ubiquitin moiety. In other models, the ubiquitin-binding domain interacts with other ubiquitinated factors important to the reaction and recruits and/or allosterically activates these factors.

The Rabex-5 A20 ZnF and IUIM system sheds new light on this question as the first example of a crystal structure in which a monoubiquitin-binding domain, a ubiquitin ligase and ubiquitin are present. The A20 ZnF-domain ubiquitin ligase presumably functions like RING-finger ubiquitin ligase as an adaptor and activator of the ubiquitin-conjugating enzyme. Thus, we can ask whether it is plausible for the IUIM and the A20 ZnF to cooperate in recruiting a ubiquitin-thiolester adduct of a Ubc. In this scenario, the IUIM would bind the ubiquitin moiety, whereas the A20 ZnF domain would bind the Ubc. The structure shows that the C terminus (with the last three residues 74–76 modeled) of the ubiquitin bound to the IUIM is 50 \AA away from the Ubc-binding site on the A20 ZnF domain. In the structure of the Cbl-UbcH7 complex³¹, there is only 15 \AA between the active site Cys86 of UbcH7 and the closest point on the RING domain, and the farthest point of the UbcH7 surface from Cys86 is only 27 \AA away. The solution of the Rabex-5 A20 ZnF-IUIM domains in four crystallographically independent states represents the modest range of flexibility between the two domains, and the range of movement is insufficient to bring the IUIM ubiquitin-binding site into proximity with the putative Ubc-binding site. This is consistent with the observation that the A58D IUIM mutation does not impair the *in vitro* ubiquitin-ligase activity of the isolated Rabex-5_{1–76} or Rabex-5_{9–73} fragment²⁸ (Fig. 6b). Therefore, simple distance constraints seem to rule out a model for the IUIM of Rabex-5 entailing direct recruitment of a Ubc monoubiquitin thiolester.

This study has shed considerable light on the little-characterized mechanism of the A20 ZnF-domain ubiquitin ligase. We have found that the A20 ZnF domain binds strongly to a novel region, the Asp58 patch, on the surface of ubiquitin. It has long been anticipated that regions of the ubiquitin surface other than Ile44 would have important

roles in ubiquitin function. This is the first description of a ubiquitin-binding domain that does not interact with the Ile44 region. The A20 ZnF domain uses the interaction between its diaromatic patch and the Asp58 patch on ubiquitin to recruit a ubiquitin-loaded Ubc. The diaromatic patch is conserved in most A20 ZnF domains, including ZnF-4 of A20 itself, which has been implicated in the ligase activity of that protein. There is a strong preference for some Ubc over others, so the recruitment is not a function of ubiquitin binding alone. The ubiquitin-A20 ZnF complex exposes considerable hydrophobic surface area to solution, including one side each of the side chains of the diaromatic patch. A model of a possible A20 ZnF-ubiquitin-E2 complex was generated by overlaying the SUMO molecule in the Ubc9-SUMO-RanGAP1-Nup358 complex³⁹ onto the A20 ZnF domain-bound ubiquitin molecule (Supplementary Fig. 2 online). The Ubc in this model is 20 \AA away from the closest point of contact with the A20 ZnF domain. However, the exposed faces of Tyr25 and Tyr26 are the closest point to the docked Ubc, and there is no apparent obstacle to a rotation of the Ubc to directly contact the A20 ZnF domain.

In summary, this study has revealed for the first time the structures of two motifs involved in ubiquitination and monoubiquitin recognition: the A20 ZnF ubiquitin ligase and the IUIM. The juxtaposition of these two domains in space explains how they carry out their individual functions autonomously at the level of the isolated domains. The A20 ZnF and IUIM, although rigidly linked, are too far apart to directly cooperate in the transfer of a single monoubiquitin moiety. The mechanism by which monoubiquitin-binding domains promote the monoubiquitination of proteins that contain them remains a major question in the field. We have moved one step closer to answering this question by ruling out one of the major potential mechanisms, direct recruitment of a Ubc ubiquitin thiolester, in the case of the Rabex-5 IUIM. By contrast, we have shown that the A20 ZnF domain immediately adjacent to the IUIM functions by just such a direct-recruitment mechanism. Conservation of the A20 ZnF sequence in other proteins suggests that A20 and other related proteins will function by a similar mechanism.

METHODS

Cloning and sample preparation. DNA coding bovine Rabex-5 residues 9–73 was subcloned into parallel GST2 vector⁴⁰. Site-directed mutants were generated using the QuikChange mutagenesis kit (Stratagene). All constructs were verified by DNA sequencing. Rabex-5_{9–73} was overexpressed as an N-terminal GST fusion protein in *Escherichia coli* BL21(DE3). ZnCl₂ was added to terrific broth media to 0.1 mM. Cells were induced with 0.5 mM IPTG and grown at 20 °C overnight. Harvested cells were lysed in 50 mM Tris-HCl (pH 7.4) and 150 mM NaCl and the supernatant was applied to a glutathione-Sepharose column (Amersham). TEV protease was used to cleave GST and was removed by passing it through TALON resin (BD Bioscience). Protein was concentrated and applied to a Superdex 200 column (Amersham) in 50 mM Tris-HCl (pH 7.4), 150 mM NaCl and 5 mM dithiothreitol. Bovine ubiquitin (Sigma) was added to the purified Rabex-5_{9–73}. The complex was purified on a Superdex 200 column and concentrated using a VivaSpin concentrator (Viva Science). All mutants were purified as just described for the wild-type protein, except that no dithiothreitol was used. DNA encoding human ubiquitin was amplified by PCR and cloned into the parallel GST2 vector. Recombinant GST and GST-ubiquitin for SPR studies were produced from BL21(DE3) cells and purified using glutathione-Sepharose affinity columns followed by Superdex S200 (GE Health Sciences) gel-filtration chromatography. GST and GST-ubiquitin samples were dialyzed against HBS-P buffer (10 mM HEPES (pH 7.4), 150 mM NaCl and 0.05% (v/v) surfactant P20).

Crystallization, data collection and structure determination. Crystals of the complex were grown in hanging drops at 22 °C. The reservoir contained 0.1 M

sodium citrate (pH 5.6), 20%–25% (w/v) PEG 4000 and 0.2 M lithium sulfate. Diffraction-quality crystals were obtained by streak seeding and were flash-frozen under liquid nitrogen. Data were collected using a Rigaku rotating anode home source and an R-AxisIV detector, and were processed with HKL2000 (HKL Research). An initial molecular-replacement solution was obtained using ubiquitin as a search model with MOLREP⁴¹ in space group $P6_1$. Solvent-flattening by the prime-and-switch algorithm in RESOLVE⁴² yielded a map (figure of merit = 0.58) that allowed us to locate the missing Rabex-5₉₋₇₃, SAD at the zinc edge, $\lambda = 1.28 \text{ \AA}$, was used to redetermine the structure of the complex and yielded a phase set with figures of merit equal to 0.36 (SOLVE⁴³) and 0.68 (RESOLVE⁴³). The structure in space group C2 was determined by molecular replacement using the $P6_1$ model. Manual model building and refinement were done using O⁴⁴ and CNS⁴⁵. For final refinement, we used REFMAC5 (ref. 46) with TLS parameters⁴⁷ incorporated (Table 2). There are no residues in disallowed regions of the Ramachandran plot. Structural figures were generated using PyMOL (<http://pymol.sourceforge.net>).

Surface plasmon resonance. The binding of wild-type and mutant Rabex-5 proteins to ubiquitin was measured with a Biacore T100 system at 25 °C with a flow rate of 20 $\mu\text{l min}^{-1}$. GST, GST-ubiquitin and GST-I44D and GST-D58A ubiquitin mutants (10,000 response units of each) were immobilized on a CM5 surface via covalent linkage to the N terminus of GST. A CM5 chip was activated using 1:1 N-hydroxysuccinimide (NHS)/1-ethyl-3-(3-dimethylaminopropyl)carbodiimide (EDC) at a flow rate of 5 $\mu\text{l min}^{-1}$ for 20 min. GST (10 μM) and GST-ubiquitin (10 μM) in 10 mM acetate buffer (pH 5.5) were passed over separate flow cells at 5 $\mu\text{l min}^{-1}$ for 40 min, and this was followed by a blocking step using ethanolamine (1 M, pH 8.5) at 5 $\mu\text{l min}^{-1}$ for 20 min. All binding experiments were performed in HBS-P. Binding of wild-type and mutant Rabex-5 proteins to ubiquitin was measured simultaneously by passing Rabex-5 over flow cells coupled to GST, GST-ubiquitin and GST-ubiquitin mutants, with association and dissociation times of 100 s and 300 s, respectively. Between subsequent injections of Rabex-5 proteins, surfaces were regenerated with an injection of HBS-P supplemented with 500 mM NaCl for 15 s at 100 $\mu\text{l min}^{-1}$.

We initially tried to fit our data assuming a 1:1 binding stoichiometry for a Rabex-5-ubiquitin complex. However, poor fitting statistics and subsequent mutational data led us to define two independent binding sites on Rabex-5 for ubiquitin, as follows:



where R is Rabex-5 and U is ubiquitin. Corresponding data were fit to the following equation:

$$R_{\text{eq}} = R_{\text{max1}}[\text{Rabex}]/([\text{Rabex}] + K_{d1}) + R_{\text{max2}}[\text{Rabex}]/([\text{Rabex}] + K_{d2}) + \text{RI}$$

where [Rabex] is the protein concentration of the flowing analyte, K_{d1} and K_{d2} are the dissociation constants for sites 1 and 2, respectively, R_{max1} and R_{max2} are the relative maximal change in response levels for sites 1 and 2, respectively, and RI is the residual or background signal. Fitting was performed using the BiaEvaluation software (Biacore) with globally floating K_d , R_{max} and RI values.

Table 2 Crystallographic data collection, phasing and refinement statistics

	Crystal A ^a	Crystal B ^a	Crystal C ^a
Data collection			
Space group	$P6_1$	$P6_1$	C2
Cell dimensions			
<i>a</i> , <i>b</i> , <i>c</i> (Å)	81.70, 81.70, 55.03	81.97, 81.97, 54.44	192.92, 44.22, 69.17
α , β , γ (°)	90, 90, 120	90, 90, 120	90, 108.98, 90
		<i>Peak</i>	
Wavelength (Å)		1.2820	
Resolution (Å)	2.95 (3.06–2.95) ^b	2.8 (2.9–2.8) ^b	2.5 (2.59–2.5) ^b
R_{sym}	0.109 (0.423)	0.073 (0.431)	0.067 (0.439)
<i>I</i> / σ <i>I</i>	27.6 (8.4)	33.8 (3.8)	24.2 (3.3)
Completeness (%)	99.8 (100.0)	95.7 (77.1)	98.8 (95.6)
Redundancy	11.1 (11.2)	11.3 (8.6)	6.4 (5.5)
Refinement			
Resolution (Å)		2.8	2.5
No. reflections		5,005	19,257
R_{work} / R_{free}^c		0.212 / 0.268	0.228 / 0.263
No. atoms			
Protein		1,087	3,204
Ligand/ion		1	8
Water		2	19
<i>B</i> -factors			
Protein		59.5	48.2
Ligand/ion		83.7	89.0
Water		37.9	32.0
R.m.s. deviation			
Bond lengths (Å)		0.007	0.007
Bond angles (°)		1.0	1.0

^aOne crystal was used for each dataset. ^bThe values in parentheses relate to highest-resolution shells. ^c R_{free} is calculated for a randomly chosen 10% (Crystal B) or 5% (Crystal C) of reflections; the *R* factor is calculated for the remaining 90% (Crystal B) or 95% (Crystal C) of reflections.

Isothermal titration calorimetry. Rabex-5₉₋₇₃ (10–30 μM , placed in the sample cell) and bovine ubiquitin (0.3–0.75 μM , injectant) were dissolved in 50 mM Tris-HCl (pH 7.4) and 150 mM NaCl. Titrations (42 injections of 5 μl ubiquitin each) were performed at 30 °C using a VP-ITC Microcalorimeter (MicroCal), and data were analyzed using Origin software (Origin Lab).

Interaction with ubiquitin-conjugating enzymes. UbcH5C was expressed using the plasmid pET15-UbcH5C⁴⁸. DNA encoding Ube2g2 was subcloned into the NcoI and BamHI sites of pET15. Human gp78 encodes a specific Ube2g2-binding site between residues 574 and 643. A fragment encoding gp78 residues 574–643 was described previously⁴⁹, as was the GST-RNF25_{86–363} construct³⁷. ³⁵S-labeled UbcH5C and Ube2g2 were translated *in vitro* using the S30 T7 bacteria lysate system (Promega). For ubiquitin thiolester formation, reactions contained 12 μl Ubc translation mix, 100 nM murine E1 and 10 μg ubiquitin in 80 μl reaction buffer (20 mM Tris (pH 7.5), 100 mM NaCl, 4 mM ATP, 2 mM MgCl₂). The reactions were carried out at 30 °C for 10 min. To produce free Ubc, the same reaction conditions were used except that E1 was omitted. An aliquot containing 2 μg of GST fusion protein immobilized on glutathione-Sepharose 4B (Amersham) was incubated with 20 μl thiolester reaction mix in 100 μl of binding buffer (PBS containing 0.2% (v/v) Triton X-100 and 0.2 mM ZnCl₂) for 2 h at 4 °C with constant mixing. Equal loading of all samples was confirmed by SDS-PAGE and Coomassie blue staining (data not shown). The immobilized proteins were collected by centrifugation and washed three times with 100 bed volumes of binding buffer. The mixture was quenched in SDS sample buffer (with or without DTT), separated by SDS-PAGE and processed for visualization on a Storm PhosphorImager (Amersham).

In vitro ubiquitination assays. Reaction mixtures contained 2 μg GST fusion proteins immobilized on glutathione-Sepharose 4B (Amersham), 100 nM

recombinant murine E1 (expressed in Sf9 cells), 40 nM recombinant UbcH5C (expressed in *E. coli*), 2 μ M Flag-ubiquitin and 0.5–1 μ M ubiquitin aldehyde in a final volume of 50 ml reaction buffer (20 mM Tris (pH 7.5), 100 mM NaCl, 4 mM ATP and 2 mM MgCl₂). Reactions were incubated at 30 °C for 90 min with agitation, washed three times with 20 bed volumes of wash buffer (20 mM Tris (pH 7.5), 100 mM NaCl, 1 mM DTT) and quenched with SDS sample buffer. Samples were subjected to SDS-PAGE and immunoblotted with an antibody to Flag. The recombinant Ubcs were prepared as described in ref. 49.

Accession codes. Protein Data Bank: Coordinates have been deposited with accession codes 2FID (P₆) and 2FIF (C₂).

Note: Supplementary information is available on the Nature Structural & Molecular Biology website.

ACKNOWLEDGMENTS

We thank M. Horning and X. Zhu for outstanding technical assistance, A. Saxena and the staff of the National Synchrotron Light Source, Brookhaven National Laboratory beamline X12C for assistance with data collection and J. Kim for discussions. This research was supported by the intramural program of the NIH through the National Institute of Diabetes and Digestive and Kidney Diseases (J.H.H.), National Cancer Institute (A.M.W.) and National Institute of Child Health and Human Development (J.S.B.). M.S.K. is a PRAT fellow of the National Institute of General Medical Sciences in the NIH. Research carried out at the National Synchrotron Light Source was supported by the US Department of Energy (DOE), Division of Materials Sciences and Division of Chemical Sciences, under Contract No. DE-AC02-98CH10886.

COMPETING INTERESTS STATEMENT

The authors declare that they have no competing financial interests.

Published online at <http://www.nature.com/nsmb/>

Reprints and permissions information is available online at <http://npg.nature.com/reprintsandpermissions/>

- Segev, N. Ypt and Rab GTPases: insight into functions through novel interactions. *Curr. Opin. Cell Biol.* **13**, 500–511 (2001).
- Zerial, M. & McBride, H. Rab proteins as membrane organizers. *Nat. Rev. Mol. Cell Biol.* **2**, 107–117 (2001).
- Pfeffer, S. & Aivazian, D. Targeting RAB GTPases to distinct membrane compartments. *Nat. Rev. Mol. Cell Biol.* **5**, 886–896 (2004).
- Seabra, M.C. & Wasmeier, C. Controlling the location and activation of Rab GTPases. *Curr. Opin. Cell Biol.* **16**, 451–457 (2004).
- Burd, C.G., Mustol, P.A., Schu, P.V. & Emr, S.D. A yeast protein related to a mammalian ras-binding protein, Vps9p, is required for localization of vacuolar proteins. *Mol. Cell Biol.* **16**, 2369–2377 (1996).
- Delprato, A., Merithew, E. & Lambright, D.G. Structure, exchange determinants, and family-wide rab specificity of the tandem helical bundle and Vps9 domains of Rabex-5. *Cell* **118**, 607–617 (2004).
- McBride, H.M. *et al.* Oligomeric complexes link Rab5 effectors with NSF and drive membrane fusion via interactions between EEA1 and syntaxin 13. *Cell* **98**, 377–386 (1999).
- Gournier, H., Stenmark, H., Rybin, V., Lippe, R. & Zerial, M. Two distinct effectors of the small GTPase Rab5 cooperate in endocytic membrane fusion. *EMBO J.* **17**, 1930–1940 (1998).
- Horiuchi, H. *et al.* A novel Rab5 GDP/GTP exchange factor complexed to Rabaptin-5 links nucleotide exchange to effector recruitment and function. *Cell* **90**, 1149–1159 (1997).
- Lippe, R., Miaczynska, M., Rybin, V., Runge, A. & Zerial, M. Functional synergy between Rab5 effector Rabaptin-5 and exchange factor Rabex-5 when physically associated in a complex. *Mol. Biol. Cell* **12**, 2219–2228 (2001).
- Hicke, L. & Dunn, R. Regulation of membrane protein transport by ubiquitin and ubiquitin-binding proteins. *Annu. Rev. Cell Dev. Biol.* **19**, 141–172 (2003).
- Hochstrasser, M. Evolution and function of ubiquitin-like protein-conjugation systems. *Nat. Cell Biol.* **2**, E153–E157 (2000).
- Pickart, C.M. Mechanisms underlying ubiquitination. *Annu. Rev. Biochem.* **70**, 503–533 (2001).
- Weissman, A.M. Themes and variations on ubiquitylation. *Nat. Rev. Mol. Cell Biol.* **2**, 169–178 (2001).
- Katzmann, D.J., Odorizzi, G. & Emr, S.D. Receptor downregulation and multivesicular-body sorting. *Nat. Rev. Mol. Cell Biol.* **3**, 893–905 (2002).
- Haglund, K., Di Fiore, P.P. & Dikic, I. Distinct monoubiquitin signals in receptor endocytosis. *Trends Biochem. Sci.* **28**, 598–603 (2003).
- Di Fiore, P.P., Polo, S. & Hofmann, K. When ubiquitin meets ubiquitin receptors: a signalling connection. *Nat. Rev. Mol. Cell Biol.* **4**, 491–497 (2003).
- Hicke, L., Schubert, H.L. & Hill, C.P. Ubiquitin-binding domains. *Nat. Rev. Mol. Cell Biol.* **6**, 610–621 (2005).
- Hofmann, K. & Falquet, L. A ubiquitin-interacting motif conserved in components of the proteasomal and lysosomal protein degradation systems. *Trends Biochem. Sci.* **26**, 347–350 (2001).
- Fisher, R.D. *et al.* Structure and ubiquitin binding of the ubiquitin-interacting motif. *J. Biol. Chem.* **278**, 28976–28984 (2003).
- Polo, S. *et al.* A single motif responsible for ubiquitin recognition and monoubiquitination in endocytic proteins. *Nature* **416**, 451–455 (2002).
- Shih, S.C. *et al.* Epsins and Vps27p/Hrs contain ubiquitin-binding domains that function in receptor endocytosis. *Nat. Cell Biol.* **4**, 389–393 (2002).
- Raiborg, C. *et al.* Hrs sorts ubiquitinated proteins into clathrin-coated microdomains of early endosomes. *Nat. Cell Biol.* **4**, 394–398 (2002).
- Bilodeau, P.S., Urbanowski, J.L., Winistorfer, S.C. & Piper, R.C. The Vps27p Hse1p complex binds ubiquitin and mediates endosomal protein sorting. *Nat. Cell Biol.* **4**, 534–539 (2002).
- Shih, S.C. *et al.* A ubiquitin-binding motif required for intramolecular monoubiquitylation, the CUE domain. *EMBO J.* **22**, 1273–1281 (2003).
- Donaldson, K.M., Yin, H.W., Gekakis, N., Supek, F. & Joazeiro, C.A.P. Ubiquitin signals protein trafficking via interaction with a novel ubiquitin binding domain in the membrane fusion regulator, Vps9p. *Curr. Biol.* **13**, 258–262 (2003).
- Davies, B.A. *et al.* Vps9p CUE domain ubiquitin binding is required for efficient endocytic protein traffic. *J. Biol. Chem.* **278**, 19826–19833 (2003).
- Mattera, R., Tsai, Y.C., Weissman, A.M. & Bonifacino, J.S. The Rab5 guanine nucleotide exchange factor Rabex-5 binds ubiquitin and functions as a ubiquitin ligase through an atypical UIM and a zinc finger domain. *J. Biol. Chem.*, published online 5 January 2006 (doi:10.1074/jbc.M509939200).
- Wertz, I.E. *et al.* De-ubiquitination and ubiquitin ligase domains of A20 downregulate NF- κ B signalling. *Nature* **430**, 694–699 (2004).
- Huang, L. *et al.* Structure of an E6AP-UbcH7 complex: insights into ubiquitination by the E2–E3 enzyme cascade. *Science* **286**, 1321–1326 (1999).
- Zheng, N., Wang, P., Jeffrey, P.D. & Pavletich, N.P. Structure of a c-Cbl-UbcH7 complex: RING domain function in ubiquitin-protein ligases. *Cell* **102**, 533–539 (2000).
- Lawrence, M.C. & Colman, P.M. Shape complementarity at protein-protein interfaces. *J. Mol. Biol.* **234**, 946–950 (1993).
- Swanson, K.A., Kang, R.S., Stamenova, S.D., Hicke, L. & Radhakrishnan, I. Solution structure of Vps27 UIM-ubiquitin complex important for endosomal sorting and receptor downregulation. *EMBO J.* **22**, 4597–4606 (2003).
- Laity, J.H., Lee, B.M. & Wright, P.E. Zinc finger proteins: new insights into structural and functional diversity. *Curr. Opin. Struct. Biol.* **11**, 39–46 (2001).
- Alam, S.L. *et al.* Ubiquitin interactions of NFZ zinc fingers. *EMBO J.* **23**, 1411–1421 (2004).
- Fang, S.Y. *et al.* The tumor autocrine motility factor receptor, gp78, is a ubiquitin protein ligase implicated in degradation from the endoplasmic reticulum. *Proc. Natl. Acad. Sci. USA* **98**, 14422–14427 (2001).
- Lorick, K.L. *et al.* RING fingers mediate ubiquitin-conjugating enzymes (E2)-dependent ubiquitination. *Proc. Natl. Acad. Sci. USA* **96**, 11364–11369 (1999).
- Prag, G. *et al.* Mechanism of ubiquitin recognition by the CUE domain of Vps9p. *Cell* **113**, 609–620 (2003).
- Reverter, D. & Lima, C.D. Insights into E3 ligase activity revealed by a SUMO-RanGAP1-Ubc9-Nup358 complex. *Nature* **435**, 687–692 (2005).
- Sheffield, P., Garrard, S. & Derewenda, Z. Overcoming expression and purification problems of RhoGDI using a family of “parallel” expression vectors. *Protein Expr. Purif.* **15**, 34–39 (1999).
- Vagin, A.A. & Teplyakov, A. MOLREP: an automated program for molecular replacement. *J. Appl. Crystallogr.* **30**, 1022–1025 (1997).
- Terwilliger, T.C. Using prime-and-switch phasing to reduce model bias in molecular replacement. *Acta Crystallogr. D Biol. Crystallogr.* **60**, 2144–2149 (2004).
- Terwilliger, T.C. & Berendzen, J. Automated MAD and MIR structure solution. *Acta Crystallogr. D Biol. Crystallogr.* **55**, 849–861 (1999).
- Jones, T.A., Zou, J.Y., Cowan, S.W. & Kjeldgaard, M. Improved methods for building protein models in electron-density maps and the location of errors in these models. *Acta Crystallogr. A* **47**, 110–119 (1991).
- Brunger, A.T. *et al.* Crystallography & NMR system: A new software suite for macromolecular structure determination. *Acta Crystallogr. D Biol. Crystallogr.* **54**, 905–921 (1998).
- Murshudov, G.N., Vagin, A.A. & Dodson, E.J. Refinement of macromolecular structures by the maximum-likelihood method. *Acta Crystallogr. D Biol. Crystallogr.* **53**, 240–255 (1997).
- Winn, M.D., Isupov, M.N. & Murshudov, G.N. Use of TLS parameters to model anisotropic displacements in macromolecular refinement. *Acta Crystallogr. D Biol. Crystallogr.* **57**, 122–133 (2001).
- Jensen, J.P., Bates, P.W., Yang, M., Vierstra, R.D. & Weissman, A.M. Identification of a family of closely related human ubiquitin conjugating enzymes. *J. Biol. Chem.* **270**, 30408–30414 (1995).
- Chen, B. *et al.* The activity of a human endoplasmic reticulum-associated degradation E3, gp78, requires its CUE domain, RING fingers, and an E2-binding site. *Proc. Natl. Acad. Sci. USA* **103**, 341–346 (2006).